Journal of Intelligent Computing and Networking

https://www.ffspub.com/index.php/jicn/index

ISSN 3079-9228 (print) E-mail: jicn.office@ffspub.com



Article

Robustness Plugin for Military Target Recognition Algorithms in On-Orbit Satellite Environments

Yang LIU[†], Pengfei WANG^{**}, Shangguang WANG^{**}

School of Computer Science (National Pilot Software Engineering School), Beijing University of Posts and Telecommunications, Beijing
100876, China

†E-mail:liuy2019@bupt.edu.cn

Received: August 4, 2025 / Revised: August 10, 2025 / Accepted: August 11, 2025 / Published online: August 30, 2025

Abstract: Remote sensing satellites are vital for military operations and intelligence. Optical payloads capture high-value imagery, while Orbit Edge Computing (OEC) enables onboard deep learning for real-time processing. However, OEC faces computational constraints, addressed via model compression—yet this introduces robustness challenges. Spaceborne noise (vibrations, clouds, dust, haze) degrades image quality, causing compressed models to fail in accurate identification, severely compromising mission effectiveness. In this work, we aim to enhance the robustness of compressed models to ensure stable and reliable military-oriented orbital edge computing tasks, proposing an Adaptive Robustness Recovery Plugin (ARP). The core design of ARP includes three key components: (1) noise feature detection based on contrastive learning to accurately distinguish clean features from perturbed ones; (2) a feature restorer based on non-local means to targetedly suppress noise interference; and (3) a dynamic insertion strategy built on Noise Perturbation Intensity (NPI) to ensure the plugin is deployed at the most critical network layers. Experiments were conducted by simulating space noise on three remote sensing datasets for target recognition and ship classification: NWPU-RESISC45, HRSC-2016, and FGSC-23. Results demonstrate that under an extreme pruning rate of 99%, ARP achieves an average improvement of 3.2% in robust accuracy compared to existing baseline methods, with no significant loss in recognition accuracy on clean data. These findings validate the effectiveness of ARP in providing robustness guarantees for compressed models within resource-constrained satellite environments.

Keywords: Satellite; on-orbit computing; robustness; model pruning; image classification https://doi.org/10.64509/jicn.11.24

1 Introduction

Military Earth observation satellites collect multispectral imagery for geospatial analysis, providing valuable support for various sensing and computing applications in harsh space environments characterized by severe constraints on energy and network connectivity [1]. Visual tasks represent one of the core applications of such satellites, including military needs such as detecting ships at military bases to track their activities [2], assessing war damage [3], and enabling all-weather regional surveillance. Military satellites can collect massive volumes of Earth imagery daily, with data quantities often reaching dozens of terabytes [4]; the traditional model relies on satellite-to-ground links to transmit data back to ground stations for processing. However, satellite-to-ground communications suffer from limited capacity, insufficient stability,

and high downlink latency, making it difficult to meet the requirements of latency-sensitive military missions.

OEC emerges as a highly promising solution, enabling inspace processing of observed data and transmitting only the processed results to the ground [5]. Nevertheless, due to the dual constraints of computational capability and energy on satellites, on-orbit processing faces significant computational bottlenecks: remote sensing images from earth observation satellites are extremely large (i.e., hundreds of millions of pixels), while the on-board computing capacity of remote sensing satellites is typically less than 10 TOPS, far exceeding the processing capability of satellite-embedded hardware [6]. This bottleneck stems not only from low hardware computing power but also from limited power generation by solar panels, which makes it challenging to process all images within

[†] Corresponding author: Yang Liu

^{*}Academic Editor: Chunxiao Jiang

^{**} These authors contributed equally to this work.

^{© 2025} The authors. This article is an open access article distributed under the terms and conditions of the Creative Commons Attribution (CC BY) license (https://creativecommons.org/licenses/by/4.0/).

the energy budget. For instance, the Baoyun satellite can collect a maximum of 260 kilojoules of energy per day, of which only approximately 150 kilojoules is allocated to computing tasks. This restricts the satellite to processing only about 22% of observable high-resolution 3K satellite images [2].

Therefore, edge computing in satellite payloads must leverage lightweight algorithms and hardware-aware technologies to mitigate the constraints imposed by limited resources [7]. These measures not only enable energy-efficient processing but also facilitate real-time or near-real-time analysis of diverse application data, achieving the dual objectives of conserving power resources and enhancing execution speed. To this end, models deployed on satellites typically require lightweight compression via techniques such as pruning, distillation, and quantization [8, 9]. These compression methods can reduce the memory, computational power, and latency consumed by tasks accordingly. However, as illustrated in Figure 1, current compression algorithms [10–12] primarily focus on model accuracy while neglecting robustness—a critical factor. Experiments show that, taking pruning algorithms as an example, although traditional algorithms can maintain stable accuracy with increasing compression rates, their robust accuracy under noise interference declines sharply, rendering the models nearly unusable.

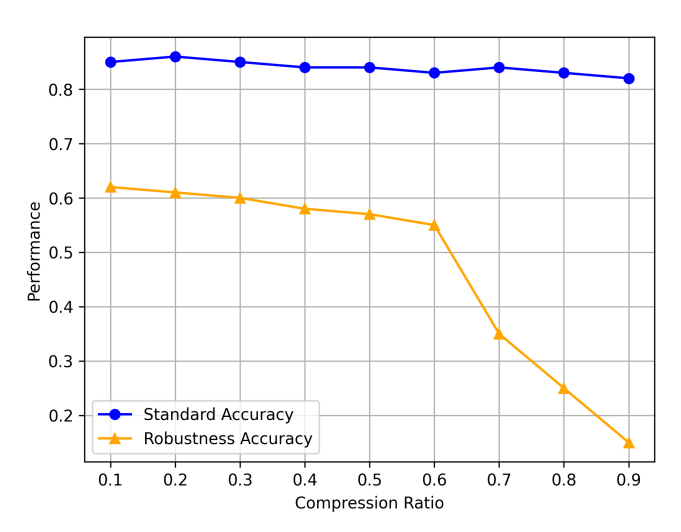


Figure 1: Performance of ResNet-18 under different robust strategies and compression ratios on the CIFAR-10 dataset. The solid line represents the performance on uncorrupted data, while the dashed line represents the performance under perturbation.

The space environment is highly dynamic and complex, with noise interference in satellite images stemming from multiple sources: the short orbital period of satellites, rapid changes in illumination conditions, combined with space vibrations and atmospheric factors (e.g., dust, haze)[13], result in substantial noise in images, which easily leads to difficulties in model recognition or misjudgment. Atmospheric dust, haze, and pollutants affect light scattering and absorption, further exacerbating the complexity of satellite image exposure. The combined effects of the space environment ultimately cause satellites to frequently capture images with limited spatial and spectral resolution, making on-orbit computing for military satellites an arduous challenge.

To address this issue, one solution is to implement image enhancement techniques to continuously acquire high-quality satellite data. For instance, improving brightness, contrast, and sharpness while preserving image details and reducing noise can enhance the accuracy of scenarios such as moving target tracking [14] and cloud coverage reduction [15] in satellite edge computing tasks. However, such solutions suffer from high costs, the need for separate deployment of image enhancement algorithms, and poor timeliness.

Another solution is to enhance the robustness of compressed models to resist noise interference, such as adversarial training [16–22], robust regularization [23–27], and robustness-aware compression strategies [28–34]. These methods improve model adaptability to specific noises by generating adversarial samples that simulate noise, but they face issues such as high training costs, difficulty in balancing regularization intensity, and increased compression complexity. These methods are difficult to adapt to the resource constraints under satellite conditions and have obvious limitations in improving the robustness of on-board compression models.

Thus, in satellite environments with limited computational resources, enabling compressed models to accurately process remote sensing images subject to heavy noise interference without consuming excessive computational power, while ensuring the stability of on-orbit tasks to provide precise and rapid military intelligence, remains an extremely challenging task.

This paper proposes a method to restore the robustness of compressed models, aiming to significantly improve the image quality and accuracy of edge computing applications, particularly in tasks such as identifying and classifying military ships. Specifically, we develop an Adaptive Robustness Recovery Plugin (ARP) to restore the robustness of compressed models. The plugin constructs a noise feature detector via contrastive learning to accurately distinguish clean features from perturbed ones; it then employs a non-local mean-based feature restorer to targetedly suppress noise interference, thereby eliminating the impact of noise on model performance. Additionally, the pre-designed plugin is precisely embedded into the optimal position within the model based on Noise Perturbation Intensity (NPI), minimizing the impact on the original model while restoring robustness. To validate the performance of the proposed method, comparative experiments are conducted using three different datasets and seven advanced algorithms under simulated space noise conditions, with results fully demonstrating its effectiveness. In summary, the main contributions of this paper are as follows:

- We address the critical issue of compressed models failing to withstand spaceborne noise in intelligent satellite observation tasks, which renders the models unusable. Specifically, we introduce an adaptive robustness plugin that achieves robustness recovery for various intelligent observation models in a loosely coupled manner.
- Our approach leverages contrastive learning for noise feature detection to accurately distinguish clean features from perturbed ones. We design a non-local means-based feature repair module to selectively suppress noise interference

and construct a dynamic insertion strategy based on Noise Perturbation Intensity (NPI) to ensure the plugin is deployed at the most critical network layers. After fine-tuning with the compressed model, we enhance overall robustness by fostering synergistic integration among these plugins.

 Extensive experiments under simulated spaceborne noise conditions validate the effectiveness of the proposed method.

2 Related Work

2.1 Remote Sensing Image Enhancement

Extensive research efforts have been devoted to advancing remote sensing image enhancement techniques. Conventional image processing methodologies encompass a range of approaches including both linear and nonlinear transformations, histogram equalization [35], Retinex theory [36], frequency-domain analysis, image fusion, and dehazing algorithms [37]. Among these, edge computing-oriented enhancement techniques rooted in traditional image processing paradigms have been developed, such as Morphological Reconstruction-based Contrast Limited Adaptive Histogram Equalization (MR-CLAHE) [38] and low-light image enhancement utilizing camera response models [39], both of which fundamentally rely on histogram equalization and Retinex theory.

While these methods demonstrate certain effectiveness in specific scenarios, they exhibit inherent limitations that constrain their practical application. The primary drawbacks include the necessity for deploying additional image enhancement algorithms, resulting in complex processing pipelines with multiple interdependent steps [14]. This computational complexity significantly impacts the real-time performance of these systems, rendering them less suitable for time-sensitive applications or resource-constrained environments. Furthermore, the cascaded nature of these algorithms often leads to cumulative errors and artifacts throughout the processing chain, potentially degrading rather than enhancing the final image quality in certain operational conditions.

2.2 Enhancing Robustness of Compressed Models

The improvement of robustness in compressed neural networks represents a critical frontier in efficient deep learning, currently addressed through three synergistic approaches [10]: architectural modifications, training paradigm innovations, and post-compression enhancements [16–22, 40, 41]. Architecturally, the integration of noise-resistant operations (e.g., non-local means filters) and perturbation-aware attention mechanisms complements robust feature extraction via depthwise separable convolutions. Training methodologies leverage compression-aware adversarial perturbations, quantization-robust loss objectives, and knowledge distillation from full-precision teacher models [23-27]. Postcompression, dynamic inference path selection based on input SNR, layer-wise feature denoising modules, and adaptive precision adjustment (e.g., 4/8-bit hybrid quantization) further sustain robustness. State-of-the-art implementations demonstrate that properly optimized compressed models can achieve full-precision-equivalent robustness with marginal computational overhead (15%), though challenges persist under extreme compression ratios (90%) or compound noise scenarios combining sensor noise, atmospheric interference, and adversarial perturbations [28–34].

3 Methods

3.1 Problem Formulation

In this subsection, we first introduce the formulation of the robust recovery problem for compressed models.

Let (\mathbf{x},y) denote an instance in the dataset, where \mathbf{x} represents the input data and y is the corresponding label. We use $f_{\boldsymbol{\theta}}(\mathbf{x})$ to denote a general compressed classifier with parameters $\boldsymbol{\theta}$, and introduce Ω to represent the additional parameters for restoring the robustness of $f_{\boldsymbol{\theta}}(\cdot)$. Here, $\delta>0$ is the perturbation radius, and x' denotes the perturbed data, which is constrained within the ℓ_{∞} -norm ball centered at x with radius δ , defined as $\mathcal{B}(x,\delta)=\{x':\|x-x'\|_{\infty}\leq\delta\}$. With these definitions, the task of robustness recovery can be formally stated as follows:

$$\min_{\mathbf{\Omega}} \sum_{(\mathbf{x}, \mathbf{y})} \left[\max_{\mathbf{x} \in \mathcal{B}(\mathbf{x}, \boldsymbol{\delta})} \mathcal{L}(f_{\theta + \mathbf{\Omega}}(\mathbf{x} + \boldsymbol{\delta}), \mathbf{y}) \right]. \tag{1}$$

3.2 Adaptive Robustness Plugin

In this subsection, we present in detail the **Adaptive Robustness Restoration Plugin (ARP)**, whose architecture is illustrated in Figure 2.

Let $\mathbf{Z}_i \in \mathbb{R}^{W_i \times H_i \times D_i}$ denote the features extracted from the i-th layer of the compressed model, where D_i represents the number of channels, and W_i and H_i correspond to the width and height of individual hidden features, respectively. Each $\mathbf{Z}_{i,j} \in \mathbb{R}^{W_i \times H_i}$ represents the feature map of the j^{th} channel in layer i. Furthermore, let \mathbf{Z}_i and $\tilde{\mathbf{Z}}_i$ denote the feature maps extracted from clean and noisy images, respectively. For each feature, we generate a binary label vector $\mathbf{y}_i' \in \{0,1\}^D$, where $\mathbf{y}_{i,j}' = 0$ indicates a feature channel significantly perturbed by noise, and $\mathbf{y}_{i,j}' = 1$ represents a noise-free feature channel from clean images.

$$Z_{ij} = \frac{1}{\mathscr{C}(\tilde{Z}_{ij})} \sum_{\forall k \in \mathscr{S}} f(\tilde{Z}_{ijh}, \tilde{Z}_{ijk}) \cdot \tilde{Z}_{ijk}, \tag{2}$$

where $f(z_{ijh},z_{ijk})$ is a feature-dependent weighting function and $\mathscr{C}(z_{ij})$ is the normalization factor. Following [42], we adopt a Gaussian (softmax) formulation: Let $f(z_{ijh},z_{ijk})=\exp\left(\frac{1}{\sqrt{d}}\theta(z_{ijh})^T\phi(z_{ijk})\right)$, where $\theta(z_{ijh})$ and $\phi(z_{ijk})$ represent two embedded representations of z_{ijh} and z_{ijk} (obtained via two 1×1 convolutions), d denotes the number of channels, and $\mathscr{C}=\sum_{\forall k\in\mathscr{S}}f(z_{ijh},z_{ijk})$. Note that f/\mathscr{C} corresponds to the softmax function, and [43] has demonstrated that this formulation is equivalent to the softmax-based self-attention computation in [44]. In order to enable the plugin to have the ability to identify clean channels and channels severely disturbed by noise, during training, we introduce a contrastive loss $\mathscr{L}_{\text{Contrast}}$ that aims to maximize the distance between feature representations of clean and perturbed images. This

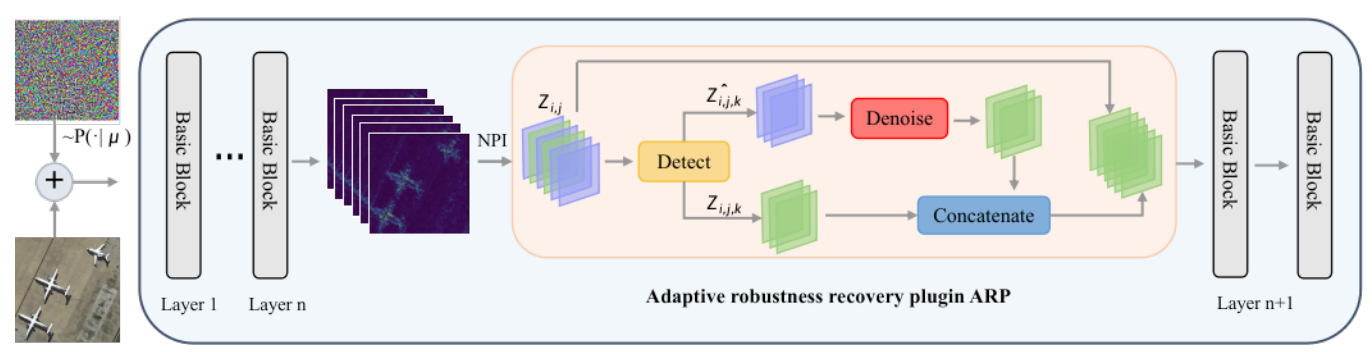


Figure 2: An overview of Adaptive Robustness Restoration Plugin (ARP).

enhances the generator's ability to discriminate meaningful differences between features, thereby improving the accuracy of ARP in identifying perturbed features. The training objective also includes a binary cross-entropy loss \mathcal{L}_{BCE} to supervise the outputs based on the generated binary labels. The total loss function $\mathscr L$ combines these two losses with a balancing weight $\lambda,$ defined as:

$$\mathcal{L} = \mathcal{L}_{BCE} + \lambda \cdot \mathcal{L}_{Contrast}, \tag{3}$$

where \mathcal{L}_{BCE} and $\mathcal{L}_{Contrast}$ are respectively defined as follows, with γ being a hyperparameter that controls the minimum distance threshold between feature representations of clean and perturbed images:

$$\mathcal{L}_{Contrast} = -\frac{1}{D_i} \sum_{j=1}^{D_i} \left(y'_{i,j} \log(p_{i,j}) + (1 - y'_{i,j}) \log(1 - p_{i,j}) \right), \tag{4}$$

$$\mathcal{L}_{\text{Contrast}} = \lambda \cdot \max \left(0, \gamma - \| \mathbf{Z}_{i,j} - \tilde{\mathbf{Z}}_{i,j} \|_{2}^{2} \right). \tag{5}$$

Based on the detector's output, the most severely perturbed channel features are fed into the feature restoration module, which operates on the principle of non-local means (NLM) smoothing [45]. The NLM algorithm computes the denoised feature map y from the input feature map x by taking a weighted average over all spatial positions \mathcal{L} , formulated as:

Through this training paradigm, the detector learns to accurately capture the intrinsic differences between perturbed and clean features, performing channel-wise classification between them. Features identified as perturbed are selectively routed to the restoration module for non-local means smoothing. This architecture offers dual advantages: (1) it effectively suppresses noise propagation within the ARP while perfectly preserving clean feature information, ensuring the original compressed model's performance remains unaffected by the additional components; (2) when encountering information perturbations, the model can intelligently identify and filter out noise before propagating features downstream, thereby guaranteeing reliable robustness restoration accuracy.

Since different model layers exhibit varying degrees of noise perturbation, the optimal plugin insertion positions can be determined by quantifying the Noise Perturbation Intensity (NPI) at each layer. For the feature map \mathbf{Z}_i at layer i, its NPI is defined as the divergence between the original and perturbed features, weighted by the feature's informational importance:

$$NPI_i = KL(P_{\mathbf{Z}_i} || P_{\tilde{\mathbf{Z}}_i}) \times || \mathbf{Z}_i ||_2^2,$$
(6)

where \mathbf{Z}_i denotes the original features at layer i, $\tilde{\mathbf{Z}}_i$ represents the noise-perturbed features, and $\|\mathbf{Z}_i\|_2^2$ measures the feature's information richness through its squared L2-norm. A higher NPI_l value indicates both greater noise corruption and higher informational significance of the layer's features, thus warranting stronger necessity for plugin insertion. In our experiments, we establish a threshold τ such that when $\mathrm{NPI}_l \geq \tau$ for a given layer, the plugin is inserted to perform targeted noise suppression.

4 Experiment

In this section, we evaluate our proposed **ARP** against several state-of-the-art methods. We first describe the experimental hardware, datasets, baseline methods, and evaluation metrics, followed by a comprehensive analysis of the results.

4.1 Heterogeneous Hardware

A computational military satellite can enhance onboard sensing, communication, and control operations. In this context, the test satellite is equipped with two industrial-grade low-power modules: Raspberry Pi 4B (RPI4) and Atlas 200 DK (Atlas). This study focuses on characterizing the onboard computing performance using these two modules, which represent widely adopted computing hardware in satellite applications.

4.2 Datasets

We conduct experiments on three publicly available real-world remote sensing datasets: NWPU-RESISC45[46], HRSC-2016[47], and FGSC-23[48].

The NWPU-RESISC45 dataset is a benchmark dataset for remote sensing image classification, comprising 256×256 pixel images distributed across 45 distinct categories. These categories encompass urban features (e.g., airports, commercial areas, and stadiums) as well as natural landscapes (e.g., forests, deserts, and wetlands).

HRSC-2016 is a ship detection dataset containing 2,976 ship instances categorized into 4 major classes and 19 fine-grained subclasses. All images were collected from six major ports, with ship sizes ranging from 300 to 1,500 pixels and spatial resolutions between 0.4m and 2m.

FGSC-23 features high-resolution ship targets captured by Google Earth and GF-2 satellite imagery over water surfaces. This fine-grained ship recognition dataset contains 4,052 instances across 23 categories, specifically designed for detailed ship identification in optical remote sensing imagery.

For all three datasets, we adopt the following data partitioning: 70% of images per class are allocated for training, 15% for validation (hyperparameter tuning), and the remaining 15% for performance evaluation.

4.3 Baseline Methods

We employ four representative methods as performance benchmarks, including:

- Two image enhancement approaches: MR-CLAHE [38] and RETINEX [36]
- Two pruning-based robustness enhancement methods: RADMM [28], HYDRA [29], PPRP [40], LM [41]. Among them, LM and PPRP are feature-level denoising methods.

4.4 Noise Simulation

We simulate noise perturbations using the methodology from [49] to evaluate model robustness under spaceborne conditions. Following Hendrycks et al. [50], we generate specialized noise types designed to emulate space-specific environmental interference: Gaussian, Poisson, and salt-and-pepper noise simulate sensor-native noise and random disturbances from rapid illumination changes; Gaussian blur and motion blur replicate scattering/absorption effects caused by atmospheric dust, haze, and satellite vibration; additionally, we include l_{∞} -bounded perturbations and other common corruptions. The robustness accuracy is computed across all corruption types and severity levels for comprehensive evaluation.

4.5 Parameter Settings

We first process remote sensing images with noise simulation to replicate space interference conditions, then perform model training and pruning to obtain compressed models. Following standard configurations [51], we train ResNet-18 and VGG-16 for 110 epochs with an initial learning rate of 0.1, which decays by a factor of 10 at epochs 100 and 105. Subsequently, we prune the weight parameters of each Conv2D layer in ResNet-18 and VGG-16 to derive compressed models. Training parameters of ARP is in Table 1:

Table 1: ARP Training Parameters Setting

Component	Parameter	Value	
ARP Training	Optimizer	SGD	
	Batch Size	128	
	Initial LR	1×10^{-4}	
	Momentum	0.9	
	Weight Decay	1×10^{-4}	

4.6 Results and Comparison

We evaluate our model on three datasets: NWPU-RESISC45, HRSC2016, and FGSC-23, using both ResNet-18 and VGG-16 architectures. Experiments conducted at pruning rates of 90%, 95%, and 99% reveal key observations (Table 2): (1) RETINEX demonstrate inferior performance, highlighting the limitations of relying solely on subnetworks to address the complex architecture-robustness relationship; (2) MR-CLAHE that incorporate robustness information during pruning achieve robustness gains but sacrifice baseline accuracy; (3) Parallel approaches (RADMM, HYDRA, LM, PPRP) show competitive performance but suffer from algorithmic complexity and high training costs. Our proposed **ARP** method achieves superior robustness across all datasets under high compression rates, effectively restoring compressed model robustness without compromising clean data accuracy.

4.7 ARP's Computational and Memory Overhead

We conducted rigorous performance measurements under simulated spaceborne noise conditions using the FGSC-23 dataset and ResNet-18 base model to evaluate ARP's operational feasibility for orbital edge computing. As shown in Table 3, the results demonstrate ARP's exceptional suitability for resource-constrained satellite environments:

Parameter Efficiency: ARP introduces only 62,976 parameters, representing just 0.54% of ResNet-18's 11.7M parameters. This extreme parameter efficiency enables deployment even on memory-constrained satellite processors.

Computational Overhead: ARP's 12.7 MFLOPS represents only 0.7% of the base model's 1,814 MFLOPS. The plugin's operations are concentrated in specific layers (conv3_x) to minimize impact.

Memory Footprint: With 0.24MB memory requirement, ARP uses just 0.27% of the base model's 89.1MB. Fixed memory allocation ensures predictable resource usage during satellite operations.

Latency Impact: On Raspberry Pi 4B: Adds 4.2ms (21.9% of base 19.2ms). On Atlas 200 DK: Adds 1.8ms (22.0% of base 8.2ms). Total inference time remains under real-time constraints for orbital applications.

5 Conclusion

The proposed model demonstrates remarkable robustness and scalability in edge computing-based satellite image deep learning, offering valuable insights for the field. It maintains stable performance for remote sensing classification and recognition tasks under both computational resource constraints and challenging spaceborne noise conditions. The model's scalability is further evidenced by its adaptability to various edge computing platforms and efficient utilization of limited computational resources. This synergistic combination of operational robustness and scalable framework, coupled with its modular design, establishes an ideal solution for on-orbit computing. The methodology is poised to advance space-based integrated observation systems and onboard data processing/decision-making capabilities.

Table 2: Performance of different models on FGSC-23, HRSC-2016 and NWPU-RESISC45 datasets at various pruning ratios. The values before the slash (/) represent clean accuracy, while the values after the slash represent robust accuracy. All values are expressed as percentages without the % symbol. Best performance is written in bold. ▲% refers to the absolute performance gain against the best baseline.

Model		ResNet-18			VGG-16		
Pruni	ng Ratio	90%	95%	99%	90%	95%	99%
	RADMM	80.54/43.68	79.33/42.56	71.17/37.21	74.76/39.92	72.67/38.44	65.69/31.30
	HYDRA	76.74/43.34	76.16/42.45	72.21/38.80	78.31/43.81	76.58/42.61	70.59/35.56
	LM	64.12/28.21	62.01/27.83	56.90/18.94	63.39/29.93	62.76/25.80	51.65/24.62
FGSC-23	PPRP	67.01/28.21	65.90/29.12	55.80/21.07	66.28/32.88	60.87/27.34	50.76/24.10
	MR-CLAHE	77.34/41.73	75.16/40.49	70.24/38.19	74.84/40.62	72.45/39.42	60.36/34.52
	RETINEX	77.39/41.31	73.54/39.29	59.42/31.37	75.66/39.26	69.27/38.27	58.49/31.24
	Ours	83.00/50.78	81.34/48.52	77.05/44.94	80.36/47.60	78.33/45.70	73.50/42.78
	▲ %	2.31/4.29	2.01/2.42	1.65/2.92	2.05/3.65	1.75/1.23	2.01/2.29
	RADMM	66.56/30.21	63.34/29.57	52.45/22.61	65.85/31.87	59.45/29.76	52.23/26.65
HRSC-2016	HYDRA	64.45/29.20	65.34/28.34	57.23/19.36	64.56/28.07	61.95/26.86	51.34/25.77
	LM	64.12/28.21	62.01/27.83	56.90/18.94	63.39/29.93	62.76/25.80	51.65/24.62
	PPRP	67.01/28.21	65.90/29.12	55.80/21.07	66.28/32.88	60.87/27.34	50.76/24.10
	MR-CLAHE	63.06/28.18	61.90/27.32	56.05/20.73	63.58/30.94	61.93/27.04	50.51/22.23
	RETINEX	65.34/28.45	64.23/27.27	56.12/18.41	62.65/27.25	57.54/25.25	50.43/24.65
	Ours	69.52/33.45	68.22/31.40	59.56/24.73	68.67/34.31	65.80/32.46	55.66/28.30
	▲ %	2.51/3.24	2.32/1.83	2.33/2.12	2.39/2.65	3.04/1.23	3.43/1.65
	RADMM	72.56/34.21	71.34/33.57	65.45/29.61	71.85/36.87	64.45/31.76	60.23/28.65
RESISC45	HYDRA	71.45/33.20	70.34/32.34	63.23/28.36	67.56/36.07	63.95/32.86	59.34/25.77
	LM	68.12/30.21	67.01/29.83	60.90/25.94	65.39/35.93	59.76/32.80	55.65/29.62
	PPRP	70.01/33.21	65.90/32.12	61.80/29.07	69.98/36.88	60.87/34.34	58.76/27.10
	MR-CLAHE	70.94/31.22	68.34/30.68	63.25/25.34	68.26/35.41	66.15/33.54	58.26/24.61
	RETINEX	72.34/32.45	69.23/31.27	59.12/27.41	71.65/33.25	64.54/31.25	61.43/27.65
	Ours	74.52/37.45	72.22/35.40	67.56/30.73	73.67/38.31	67.98/36.46	64.66/31.30
	▲ %	2.51/3.24	2.32/1.83	2.33/2.12	1.82/1.43	3.44/2.12	3.23/1.68

Table 3: Computational and Memory Overhead Analysis

Method	Parameters	Ops (MFLOPS)	Memory (MB)	Overhead (%)	Latency (ms)
BaseModel	11,689,512	1,814	89.1	_	19.2/8.2
ARP	62,976	12.7	0.24	0.7	4.2/1.8

Funding

This work is supported by the National Natural Science Foundation of China under Grant 62372059, and the Innovation Talent Fund of Beijing University of Posts and Telecommunications under Grant 2023ZCJH07.

Author Contributions

Conceptualization, Pengfei Wang and Shangguang Wang; methodology, Pengfei Wang and Yang Liu; software, Yang Liu; validation, Yang Liu, Pengfei Wang and Shangguang Wang; formal analysis, Yang Liu; investigation, Yang Liu; resources, Shangguang Wang; data curation, Pengfei Wang; writing—original draft preparation, Yang Liu and Pengfei Wang; writing—review and editing, Yang Liu; visualization,

Yang Liu; supervision, Shangguang Wang; project administration, Shangguang Wang; funding acquisition, Pengfei Wang. All authors have read and agreed to the published version of the manuscript.

Conflict of Interest

All the authors declare that they have no conflict of interest.

Data Available

The data and materials used in this study are availableupon request from the corresponding author.

References

- [1] Denby, B., Lucia, B.: Orbital edge computing: Machine inference in space. IEEE Computer Architecture Letters **18**(1), 59–62 (2019) https://doi.org/10.1109/LCA.2019. 2907539
- [2] Zhang, Q., Yuan, X., Xing, R., Zhang, Y., Zheng, Z., Ma, X., Xu, M., Dustdar, S., Wang, S.: Resourceefficient in-orbit detection of earth objects. In IEEE INFOCOM 2024 - IEEE Conference on Computer Communications, pp. 551–560 (2024). https://doi.org/ 10.1109/INFOCOM52122.2024.10621328
- [3] Holail, S., Saleh, T., Xiao, X., Xiao, J., Xia, G.-S., Shao, Z., Wang, M., Gong, J., Li, D.: Time-series satellite remote sensing reveals gradually increasing war damage in the gaza strip. National Science Review 11(9), 304 (2024)
- [4] Ramapriyan, H.: The Role and Evolution of NASA's Earth Science Data Systems. (2015). https://ntrs.nasa.gov/citations/20150018076
- [5] Denby, B., Lucia, B.: Orbital edge computing: Nanosatellite constellations as a new class of computer system. In Proceedings of the Twenty-Fifth International Conference on Architectural Support for Programming Languages and Operating Systems, pp. 939–954 (2020)
- [6] Wang, G., Wan, G., Su, Z., Wang, Y., Jia, Y., Li, G., Liang, S.: High-performance on-orbit intelligent computing and real-time services for remote sensing satellites based on large-scale computing power in space. IEEE Access 13, 92114–92133 (2025)
- [7] Pi, Y., Yang, B., Li, X., Wang, M.: Study of full-link onorbit geometric calibration using multi-attitude imaging with linear agile optical satellite. Optics Express **27**(2), 980–998 (2019)
- [8] Deng, L., Li, G., Han, S., Shi, L., Xie, Y.: Model compression and hardware acceleration for neural networks: A comprehensive survey. Proceedings of the IEEE 108(4), 485–532 (2020)
- [9] Lopes, A., Santos, F., Oliveira, D., Schiezaro, M., Pedrini, H.: Computer vision model compression techniques for embedded systems: A survey. Computers & Graphics 123 (2024) https://doi.org/10.1016/j.cag.2024. 104015
- [10] Han, S., Pool, J., Tran, J., Dally, W.: Learning both weights and connections for efficient neural network. In Advances in Neural Information Processing Systems 28 (NIPS 2015), pp. 1–9 (2015)
- [11] Guo, Y., Yao, A., Chen, Y.: Dynamic network surgery for efficient dnns. In Advances in Neural Information Processing Systems 29 (NIPS 2016), pp. 1–9 (2016)

- [12] Lee, N., Ajanthan, T., Torr, P.H.S.: Snip: single-shot network pruning based on connection sensitivity. In 7th International Conference on Learning Representations, pp. 1–15 (2019)
- [13] Li, Q., Wang, S., Ma, X., Zhou, A., Yang, F.: Towards sustainable satellite edge computing. In 2021 IEEE International Conference on Edge Computing (EDGE), pp. 1–8 (2021). IEEE
- [14] Bui, T.-A., Lee, P.-J., Liang, C.-S., Hsu, P.-H., Shiu, S.-H., Tsai, C.-K.: Edge-computing-enabled deep learning approach for low-light satellite image enhancement. IEEE Journal of Selected Topics in Applied Earth Observations and Remote Sensing 17, 4071–4083 (2024) https://doi.org/10.1109/JSTARS.2024.3357093
- [15] Tritscher, I., Pitts, M.C., Poole, L.R., Alexander, S.P., Cairo, F., Chipperfield, M.P., Grooß, J.-U., Höpfner, M., Lambert, A., Luo, B., *et al.*: Polar stratospheric clouds: Satellite observations, processes, and role in ozone depletion. Reviews of geophysics **59**(2), 1–81 (2021)
- [16] Silva, S.H., Najafirad, P.: Opportunities and challenges in deep learning adversarial robustness: A survey. arXiv preprint arXiv:2007.00753 (2020)
- [17] Dettmers, T., Zettlemoyer, L.: Sparse networks from scratch: Faster training without losing performance. arXiv preprint arXiv:1907.04840 (2019)
- [18] Özdenizci, O., Legenstein, R.: Training adversarially robust sparse networks via bayesian connectivity sampling. In International Conference on Machine Learning, pp. 8314–8324 (2021). PMLR
- [19] Vemparala, M.-R., Fasfous, N., Frickenstein, A., Sarkar, S., Zhao, Q., Kuhn, S., Frickenstein, L., Singh, A., Unger, C., Nagaraja, N.-S., *et al.*: Adversarial robust model compression using in-train pruning. In Proceedings of the IEEE/CVF Conference on Computer Vision and Pattern Recognition, pp. 66–75 (2021)
- [20] Vemparala, M.R., Fasfous, N., Frickenstein, A., Sarkar, S., Zhao, Q., Kuhn, S., Frickenstein, L., Singh, A., Unger, C., Nagaraja, N.S., Wressnegger, C., Stechele, W.: Adversarial robust model compression using in-train pruning. In IEEE Conference on Computer Vision and Pattern Recognition Workshops, pp. 66–75. IEEE, ??? (2021). https://doi.org/10.1109/CVPRW53098.2021.00016
- [21] Özdenizci, O., Legenstein, R.: Training adversarially robust sparse networks via bayesian connectivity sampling. In Meila, M., Zhang, T. (eds.) Proceedings of the 38th International Conference on Machine Learning, vol. 139, pp. 8314–8324 (2021)
- [22] Li, C., Qiu, Q., Zhang, Z., Guo, J., Cheng, X.: Learning

- adversarially robust sparse networks via weight reparameterization. In Proceedings of the AAAI Conference on Artificial Intelligence, vol. 37, pp. 8527–8535 (2023)
- [23] Liu, Z., Sun, M., Zhou, T., Huang, G., Darrell, T.: Rethinking the value of network pruning. In 7th International Conference on Learning Representations, pp. 1–21 (2019)
- [24] Cosentino, J., Zaiter, F., Pei, D., Zhu, J.: The search for sparse, robust neural networks. arXiv preprint arXiv:1912.02386 (2019)
- [25] Li, B., Wang, S., Jia, Y., Lu, Y., Zhong, Z., Carin, L., Jana, S.: Towards practical lottery ticket hypothesis for adversarial training. arXiv preprint arXiv:2003.05733 (2020)
- [26] Fu, Y., Yu, Q., Zhang, Y., Wu, S., Ouyang, X., Cox, D., Lin, Y.: Drawing robust scratch tickets: Subnetworks with inborn robustness are found within randomly initialized networks. Advances in Neural Information Processing Systems **34**, 13059–13072 (2021)
- [27] Chen, T., Zhang, Z., Wang, P., Balachandra, S., Ma, H., Wang, Z., Wang, Z.: Sparsity winning twice: Better robust generalization from more efficient training. In The Tenth International Conference on Learning Representations, pp. 1–21 (2019)
- [28] Ye, S., Xu, K., Liu, S., Cheng, H., Lambrechts, J.-H., Zhang, H., Zhou, A., Ma, K., Wang, Y., Lin, X.: Adversarial robustness vs. model compression, or both? In 2019 IEEE/CVF International Conference on Computer Vision (ICCV), pp. 111–120 (2019). https://doi.org/10. 1109/iccv.2019.00020
- [29] Sehwag, V., Wang, S., Mittal, P., Jana, S.: Hydra: Pruning adversarially robust neural networks. In Advances in Neural Information Processing Systems 33 (NeurIPS 2020), pp. 1–12 (2020)
- [30] Lee, B.-K., Kim, J., Ro, Y.M.: Masking adversarial damage: Finding adversarial saliency for robust and sparse network. In Proceedings of the IEEE/CVF Conference on Computer Vision and Pattern Recognition, pp. 15126–15136 (2022)
- [31] Jian, T., Wang, Z., Wang, Y., Dy, J., Ioannidis, S.: Pruning adversarially robust neural networks without adversarial examples. In 2022 IEEE International Conference on Data Mining (ICDM), pp. 993–998 (2022). https://doi.org/10.1109/ICDM54844.2022.00120
- [32] Zhao, Q., Königl, T., Wressnegger, C.: Non-uniform adversarially robust pruning. In Proceedings of the International Conference on Automated Machine Learning (AutoML), pp. 1–16 (2022)
- [33] Zhao, Q., Wressnegger, C.: Holistic adversarially robust

- pruning. In The Eleventh International Conference on Learning Representations, pp. 1–22 (2023)
- [34] Thorsteinsson, H., Henriksen, V.J., Chen, T., Selvan, R.: Adversarial fine-tuning of compressed neural networks for joint improvement of robustness and efficiency. arXiv preprint arXiv:2403.09441 (2024)
- [35] Pandey, K., Singh, S.: A comparative study of histogram equalization techniques for image contrast enhancement. International Journal of Engineering Science & Advanced Technology **8**(6), 305–308 (2014)
- [36] Singh, K., Parihar, A.S.: Illumination estimation for nature preserving low-light image enhancement. The Visual Computer **40**(1), 121–136 (2024)
- [37] Wang, W., Wu, X., Yuan, X., Gao, Z.: An experiment-based review of low-light image enhancement methods. IEEE Access **8**, 87884–87917 (2020)
- [38] Lashkov, I., Yuan, R., Zhang, G.: Edge-computing-facilitated nighttime vehicle detection investigations with clahe-enhanced images. IEEE Transactions on Intelligent Transportation Systems **24**(11), 13370–13383 (2023)
- [39] Ren, Y., Ying, Z., Li, T.H., Li, G.: Lecarm: Low-light image enhancement using the camera response model. IEEE Transactions on Circuits and Systems for Video Technology **29**(4), 968–981 (2018)
- [40] Fang, J., Zhang, Z., Sun, J., Fu, J., He, H., Liu, Y., Ma, W.: Improve model robustness in less time than it takes to drink a cup of coffee with plug-and-play plugins. In Proceedings of the Asian Conference on Computer Vision, pp. 1520–1531 (2024)
- [41] Ozfatura, E., Hameed, M.Z., Ozfatura, K., Gunduz, D.: Less is more: Feature selection for adversarial robustness with compressive counter-adversarial attacks. arXiv preprint arXiv:2106.10252 (2021)
- [42] Xie, C., Wu, Y., Maaten, L.v.d., Yuille, A.L., He, K.: Feature denoising for improving adversarial robustness. In Proceedings of the IEEE/CVF Conference on Computer Vision and Pattern Recognition, pp. 501–509 (2019)
- [43] Wang, X., Girshick, R., Gupta, A., He, K.: Non-local neural networks. In Proceedings of the IEEE Conference on Computer Vision and Pattern Recognition, pp. 7794–7803 (2018)
- [44] Vaswani, A., Shazeer, N., Parmar, N., Uszkoreit, J., Jones, L., Gomez, A., Kaiser, L., Polosukhin, I.: Attention is all you need. In Advances in Neural Information Processing Systems 30 (NIPS 2017), pp. 1–11 (2017)
- [45] Salman, H., Sun, M., Yang, G., Kapoor, A., Kolter, J.Z.: Denoised smoothing: A provable defense for pretrained

- classifiers. In Advances in Neural Information Processing Systems 33 (NeurIPS 2020), pp. 21945–21957 (2020)
- [46] Cheng, G., Han, J., Lu, X.: Remote sensing image scene classification: Benchmark and state of the art. Proceedings of the IEEE **105**(10), 1865–1883 (2017)
- [47] Gwinner, K., Jaumann, R., Hauber, E., Hoffmann, H., Heipke, C., Oberst, J., Neukum, G., Ansan, V., Bostelmann, J., Dumke, A., *et al.*: The high resolution stereo camera (hrsc) of mars express and its approach to science analysis and mapping for mars and its satellites. Planetary and Space Science **126**, 93–138 (2016)
- [48] Yao, L., Zhang, X., Lyu, Y., Sun, W., Li, M.: Fgsc-23: A high-resolution optical remote sensing image ship

- target dataset for fine-grained recognition in deep learning. Journal of Image and Graphics **26**(10), 2337–2345 (2021)
- [49] Croce, F., Hein, M.: Reliable evaluation of adversarial robustness with an ensemble of diverse parameter-free attacks. In International Conference on Machine Learning, pp. 2206–2216 (2020). PMLR
- [50] Hendrycks, D., Dietterich, T.G.: Benchmarking neural network robustness to common corruptions and surface variations. arXiv preprint arXiv:1807.01697 (2018)
- [51] Madry, A., Makelov, A., Schmidt, L., Tsipras, D., Vladu, A.: Towards deep learning models resistant to adversarial attacks. In 6th International Conference on Learning Representations, pp. 1–23 (2018)